Correlation between process parameters and mechanical properties of Ti6Al4V alloys processed by electron beam melting

Carolina Schillaci, Daniela Pilone, Filippo Berto
Department of Chemical Engineering, Materials and Environment, Sapienza University of Rome, via Eudossiana 18, Rome 00184, Italy.
carolina.schillaci@uniroma1.it, https://orcid.org/0009-0006-6003-7149
daniela.pilone@uniroma1.it, https://orcid.org/0000-0002-8757-8360
filippo.berto@uniroma1.it, https://orcid.org/0000-0002-0591-0754

Costanzo Bellini, Vittorio Di Cocco
Department of Civil and Mechanical Engineering, University of Cassino and Southern Lazio, via G. Di Biasio 43, Cassino 03043, Italy.
c.bellini@unicas.it, https://orcid.org/0000-0003-4804-6588
v.dicocco@unicas.it, https://orcid.org/0000-0002-1668-3729

Paolo Di Giamberardino, Daniela Iacoviello
Dept. of Computer, Control and Management Engineering "Antonio Ruberti", Sapienza, University of Rome, 00184 Rome, Italy.
paolo.digiamberardino@uniroma1.it, https://orcid.org/0000-0002-9113-8608
daniela.iacoviello@uniroma1.it, https://orcid.org/0000-0003-3506-1455

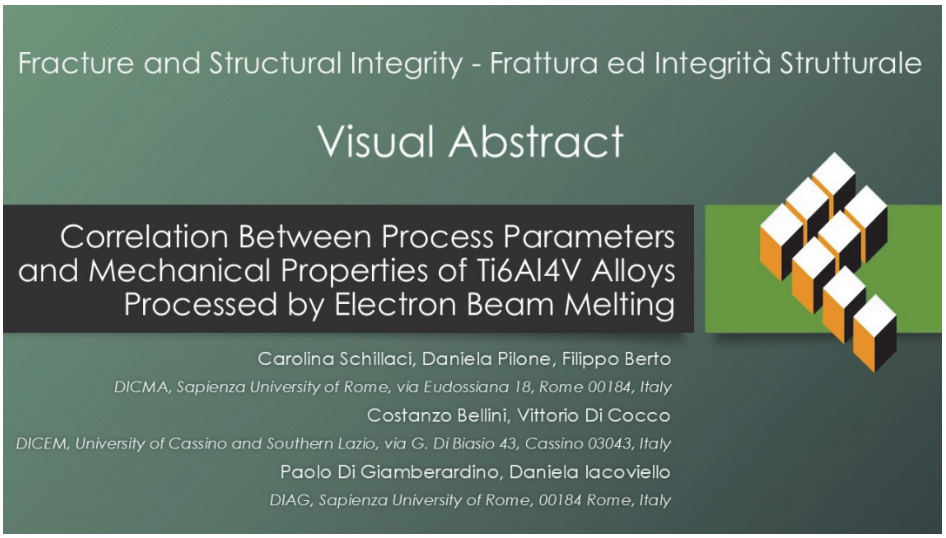

Citation: Schillaci, C., Pilone, D., Berto, F., Bellini, C., Di Cocco, V., Di Gianberardino, P., Iacoviello, D.,Correlation between process parameters and mechanical properties of Ti6Al4V alloys processed by electron beam melting, Fracture and Structural Integrity, 74 (2025) 310-320.

Received: 07.07.2025
Accepted: 12.08.2025
Published: 08.09.2025
Issue: 10.2025

KEYWORDS. Additive manufacturing, EBM process, Image analysis, Mechanical properties, Ti6Al4V alloy.

INTRODUCTION

Ti6Al4V alloys are widely utilized in aerospace, biomedical, and industrial applications due to their excellent mechanical properties, corrosion resistance, and biocompatibility. Traditionally, components made by using this alloy are manufactured using conventional techniques such as casting, forging, and machining. However, these methods often impose important design limitations and require extensive post-processing [1] to obtain the desired geometries and properties. Additive manufacturing (AM) has been emerging as an interesting alternative, offering advantages such as design flexibility, material efficiency, and the ability to fabricate complex geometries starting from simple CAD models. With this fabrication methodology product customization is easy to attain without any extra cost usually associated with conventional processing methods. Among the different AM techniques, Electron Beam Melting (EBM) is particularly effective for processing Ti6Al4V alloys due to its high-energy beam, vacuum environment, and controlled heating.

The microstructure of Ti6Al4V alloys produced by EBM differs from that of the conventionally processed ones. In fact, EBM process is characterized by a build temperature of 600-750 °C, resulting in a slow cooling rate compared to other AM techniques such as Laser Powder Bed Fusion and a stress relief treatment obtained during successive deposition cycles [2, 3]. Slow cooling rates determine the formation of columnar prior β grains that grow in the build direction and transform, during cooling, β phase into α+β lamellar structures [4]. The microstructural characteristics, including grain size, phase distribution, and texture, play a key role in determining the mechanical properties of the material and then of the component. Obtaining a refined α+β lamellar structure can improve strength and toughness, whereas coarser lamellae may lead to anisotropic mechanical behavior [5].

Although the EBM process provides advantages such as reduced residual stress and more efficient material utilization, the process can produce defects that influence the material mechanical performances [6, 7, 8]. Common defects in EBM-fabricated Ti6Al4V alloy include porosity, lack of fusion, and high surface roughness [9]. Porosity can originate from trapped gas. Gas pores are generally small (< 100 μm) and spherical, while lack of fusion defects are characterized by an irregular shape with a large aspect ratio. Keyhole pores, generated for a high energy input, are generally large and spherical. During the process, the surface roughness can be generated by melt pool hydrodynamic effects, staircase effect, and partially melted powder particle adhesion [10, 11, 12]. By increasing surface roughness fatigue life is reduced. On the other hand, when porosity influences mechanical properties, the elastic modulus and strength values are closely linked to the quantity and morphology of the pores. Total elongation is also affected by porosity, though its effect varies depending on the toughness of the alloy. The presence of lack of fusion defects, compared to other types of pores, has a more significant impact on the mechanical properties of the alloy. Additionally, the layered nature of AM processes introduces anisotropy in mechanical properties, affecting tensile strength, fatigue life, and fracture toughness [13, 14, 15, 16]. Understanding the correlation between microstructure, defects, and mechanical properties is essential for optimizing EBM parameters and enhancing the reliability of Ti6Al4V alloy components for critical applications.

The research presented in this article is part of a broader study aimed at developing a fully automated procedure, based on machine learning methods, to correlate process parameters with mechanical properties. This part of the study aims at investigating the relationship between process parameters used during EBM fabrication and Ti6Al4V alloy mechanical properties. Process parameters affect microstructural evolution, defect formation, and then mechanical performance of the alloy. By analyzing how process parameters and building direction influence microstructural features and defect size, shape and distribution, it is possible to develop strategies to enhance mechanical properties, minimize defects, and improve the overall performance of EBM-fabricated Ti6Al4V components. The findings will contribute to the advancement of additive manufacturing for high-performance titanium alloys, enabling their broader adoption in industries requiring lightweight, durable, and complex structures.

MATERIALS AND METHODS

Ti6Al4V specimens used for this study were produced by means of EBM technology. Metallic cylinders, having a diameter of 10 mm and a length of 133.6 mm have been produced by using an Arcam A2X machine. Dogbone specimens, shown in Fig.1, have been obtained by machining. EBM process is performed under vacuum to avoid the deflection of the electron beam due to its interaction with the air molecules. The EBM process has been initiated by pre-heating the powder bed using a defocused electron beam. The pre-heating temperature is 700 °C. This process step guarantees limited shrinkages and residual stress. In this study the specimens have been built layer by layer, with a layer thickness of 50 μm and a hatch spacing, which is the distance between the centers of two adjacent beams, equal to 0.1 mm.

As far as the other process parameters are concerned, the used process parameters are listed in Tab. 1. In addition to the process parameters, an additional variable has been introduced in the experimental campaign: build orientation. Half of the specimens were fabricated with their longitudinal axis oriented perpendicular to the building direction (horizontal orientation), while the remaining half have been produced with the axis parallel to the build direction (vertical orientation). In the horizontal configuration, during the mechanical test, the tensile load has been applied perpendicularly to the build direction; while, in the vertical configuration, the load has been applied parallel to the building direction. Three specimens were manufactured and tested for each unique combination of process parameters and building orientation, resulting in a total of 24 specimens for the entire test campaign.

Batch	v (mm/s)	I (mA)	h (mm)	t (mm)	V (kV)	VED* (J/mm³)
A	4530	15	0.1	0.05	60	39.7
B	6000	8	0.1	0.05	60	16.0
C	10000	15	0.1	0.05	60	18.0
D	9600	8	0.1	0.05	60	10.0

* Volumetric Energy Density

Table 1: Process parameters used to produce 4 batches of samples (A, B, C, D).

After cooling down slowly, the specimens have been removed from the powder bed using a powder recovery system, and they have been cleaned using an ultrasonic bath. A sketch of the dogbone specimens is reported in Fig.1. From this figure it is possible to observe that one of the specimen shoulders is longer. It has been designed in this way with the aim of having for each specimen a portion of material necessary for performing microstructural analyses. After the production stage, the samples taken from dogbone samples have been sectioned in two perpendicular directions: one parallel and the other one perpendicular to the building direction. The samples have been grounded by using SiC papers with a grit size ranging from 400 to 1200. Mirror finish polishing has been performed using 1 μm and 0.3 μm alumina aqueous suspension. The unetched specimens have been used to analyze the defective state of the alloy by using the Leica DMI5000 M Metallurgical Microscope. The alloy microstructure has been analyzed after etching with the Keller's reagent.

The acquired images with the same magnitude (50x), have been analyzed to extract information regarding the size, shape and density of defects. For this purpose, a Python code was written using OpenCV library [17]. Each image has been converted to grayscale, and then to binary images through a constant thresholding. Noises have been removed using morphological operations: this made the defects' detection easier. A contour detection algorithm has been used to identify the defects in the white and black images. Then defect size has been characterized by using two parameters: area and Feret diameter. The first is represented as the ratio between the total defect area per image and the total image area. The second one represents defect size along a given direction. To obtain it, each defect has been circumscribed into the minimum area rectangle, whose sides were tangent to the defects' contour. The circularity and aspect ratio were found to characterize the defects' shape. The first is defined as $4\pi \times \frac{A_{def}}{P_{def}^{\ 2}}$, where A_{def} is the area of the defect and P_{def} its perimeter. It is a value within 0 and 1, where 1 corresponds to a perfect circle. The aspect ratio is the ratio between the minor axis and the major axis of the best-fitting ellipse, in the mean square error sense, that minimizes the squared distance from each contour point to the ellipse edge. It measures the elongation of each defect and is a number that ranges between 0 and 1.

The alloy microstructure has been studied by performing X-ray diffraction with monochromatic Cu kα source. XRD analyses have been performed using a Philips PW 1830 diffractometer, equipped with a Philips X'PERT vertical Bragg–Brentano powder goniometer. Data have been collected in step-scan mode over a 2θ range of 20° to 90°, with a step size of 0.02° and a counting time of 1 second per step.

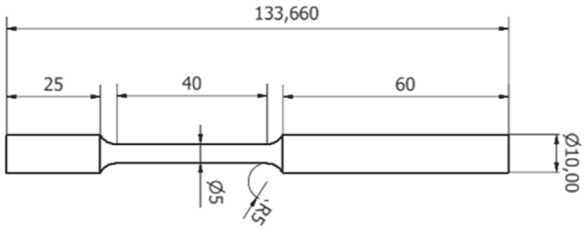

Figure 1: Sketch of the samples used for tensile tests.

RESULTS

Specimens produced by using EBM have been sectioned and analyzed to verify the alloy microstructure. X-ray diffraction pattern shown in Fig. 2 highlights that the alloy is constituted by α+β phases. In additive manufacturing processes each layer is subjected to a complex thermal cycle due to the deposition of subsequent layers. During the cooling of the melt pool the β grain solidification direction follows the temperature gradient. This justifies the formation of elongated columnar β grains [18]. The size of the columnar β grains is determined by the dwell time between the liquidus temperature and β transus temperature and then it depends on the process parameters selected during the fabrication process. When the alloy cools down α phase nucleates at the grain boundaries. When α phase nucleates at the grain boundaries and α laths nucleate within β grains the basket-weave structure forms.

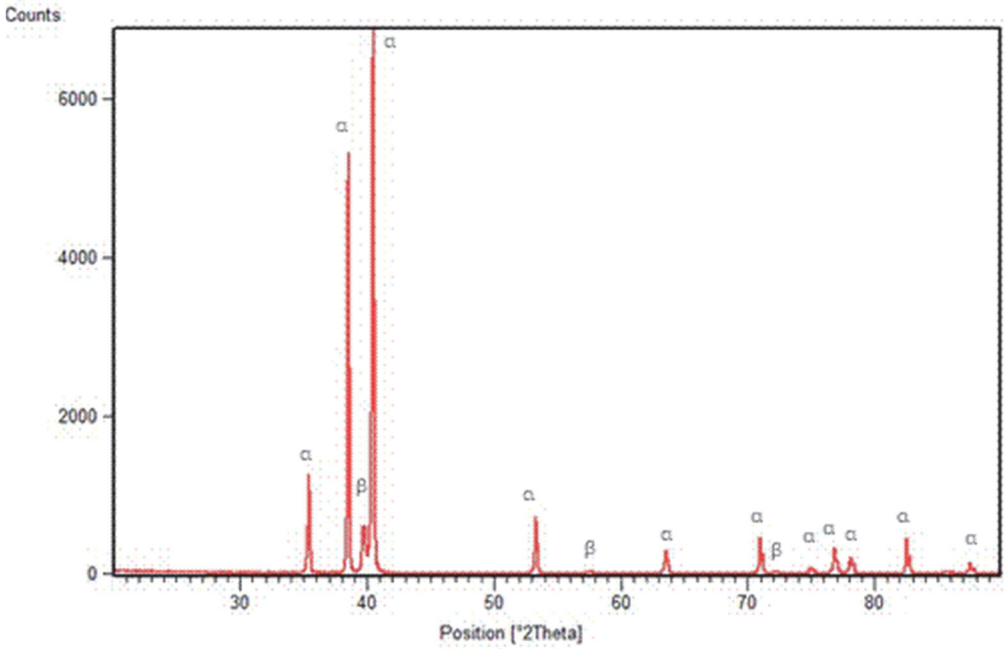

Figure 2: XRD pattern of Ti6Al4V alloy produced by EBM.

Fig. 3 shows the microstructure of Ti6Al4V alloy produced by EBM. Epitaxial prior β grains, well visible in the optical micrograph due to the formation of α phase at the prior β grains boundaries, have a thickness of about 160 μm. The alloy microstructure is characterized by the presence of α lath colonies and basket weave structure. This is justified considering that in EBM process cooling rates are in the range 10^3 to 10^5 K/s, less than that required to form martensite in Ti6Al4V alloys [19]. α laths present in the analyzed specimens have a thickness of about 1.5 μm. The mechanical properties of Ti6Al4V alloy depends on the cooling rates that affect the α lath thickness [2].

Dogbone tensile specimens were tested to determine the mechanical properties of the studied alloy in both the parallel and orthogonal directions relative to the build orientation. The curves reported in Fig.4 show the behavior of Ti6Al4V alloy loaded along the direction perpendicular to the build direction.

Specimen A, produced by using the highest volumetric energy density and predominantly characterized by the presence of circular gas defects, shows the highest value of strength and a value of elongation at break consistent with those reported in the literature [2]. By observing Fig.4 it is possible to see that B and C samples have very similar behavior and that the increased percentage of defects, due to the lower volumetric energy density in comparison with specimen A, determines stress concentration and lower strength of the material. Moreover, the presence of defects affects the Young modulus value [20]. In fact, based on the model proposed by Gibson and Ashby [21], the key structural feature that determines the mechanical behavior of a porous material is its relative density ϱ/ϱ_s, defined as the ratio of the material's density (ϱ) to that of the alloy it is made from (ϱ_s). The D specimens, fabricated using the lowest volumetric energy density, exhibited the highest percentage of defects and the most reduced mechanical properties.

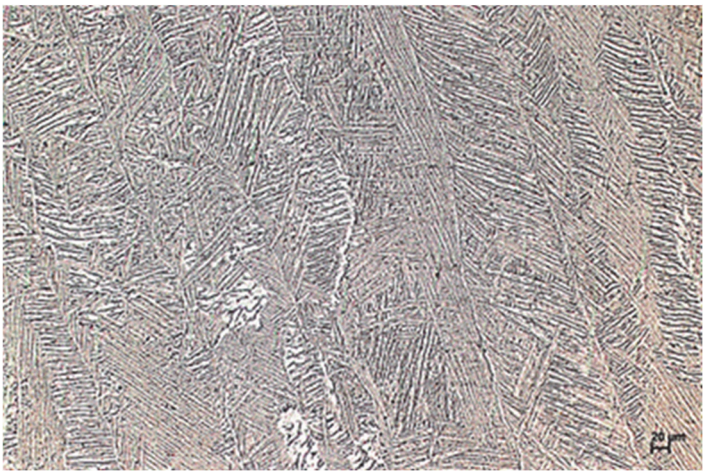

Figure 3: Microstructure of Ti6Al4V alloy (Sample A) along the longitudinal section after etching with Keller's reagent.

Fig. 5 shows stress-strain curves obtained by testing specimens loaded along the building direction. This figure highlights that, while specimens AV and AH have almost the same behavior, specimens B, C and D that contain defects, have different mechanical properties. BV, CV, and DV samples show significantly lower strength compared to the BH, CH, and DH samples. The letters H and V indicate that the specimens were manufactured with horizontal and vertical build orientations, respectively.

To explain these findings, image analysis has been performed on many micrographs. Images of cross sections along a plane parallel and perpendicular to the building direction were analyzed for each set of process parameters. Fig.6 and Fig.7 show some of the results of image analysis highlighting the Feret diameter and defect area percentage respectively, while Fig.8 and Fig.9 show the aspect ratio and circularity for all the specimens considered. In these figures, the set of process parameters is displayed along the x-axis and is represented by the first letter (A, B, C or D). The second letter indicates the sections longitudinal (L) or transversal (T) relative to the building direction.

From Fig. 7 it is possible to observe that the percentage of surface occupied by defects increases from batch A (0.015%-0.12%) to batch D (19.7%-25%), as the volumetric energy density decreases.

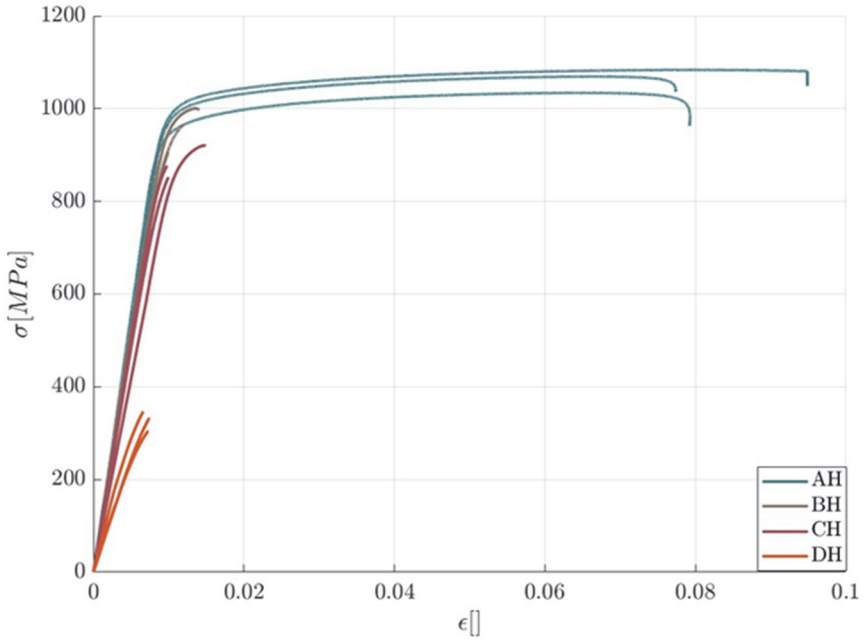

Figure 4: Stress-strain curves of specimens A, B, C, D built horizontally and loaded along the direction perpendicular to the build direction.

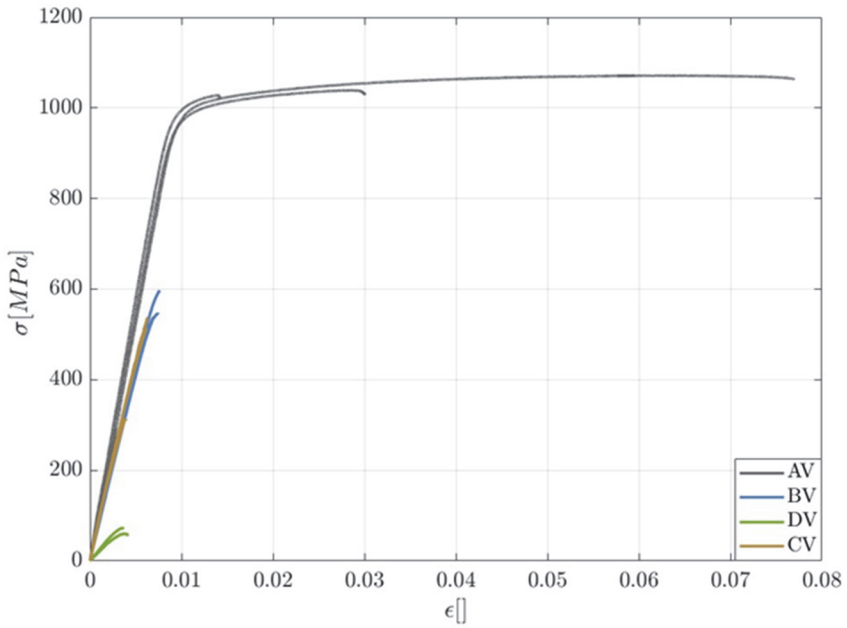

Figure 5: Stress-strain curves of specimens build vertically and loaded along the build direction.

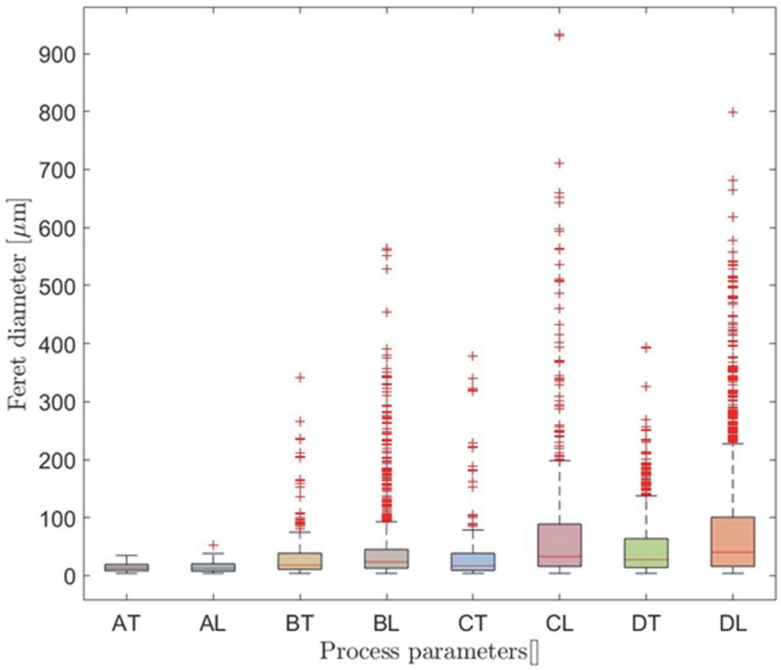

Figure 6: Feret diameter for each set of process parameters (A, B, C, and D), measured on longitudinal (L) and transverse (T) sections relative to the build direction.

Comparing longitudinal and transverse sections of batches A, B and C, the defects on transversal sections show higher circularity and aspect ratio. This suggests that the defects' orientation with respect to the loading condition during tensile tests, is more deleterious for the specimens printed vertically, as confirmed by the tensile test results.
By analyzing DT and DL, while there is only a small difference in the dataset distribution of circularity and aspect ratio, there is a notable difference in the defect area percentage (Fig. 7). It indicates that the static resistance of the specimens D printed vertically was lower than the ones printed horizontally due to the defect size and to the stress intensification due to the low defect curvature radius. Although batches B and C were produced using the same VED, some differences can still

be observed. The boxplot data for CT indicates a higher quantity of small and circular defects, compared to BT. It can be attributed to a higher quantity of gas pores, as shown on Fig.10.

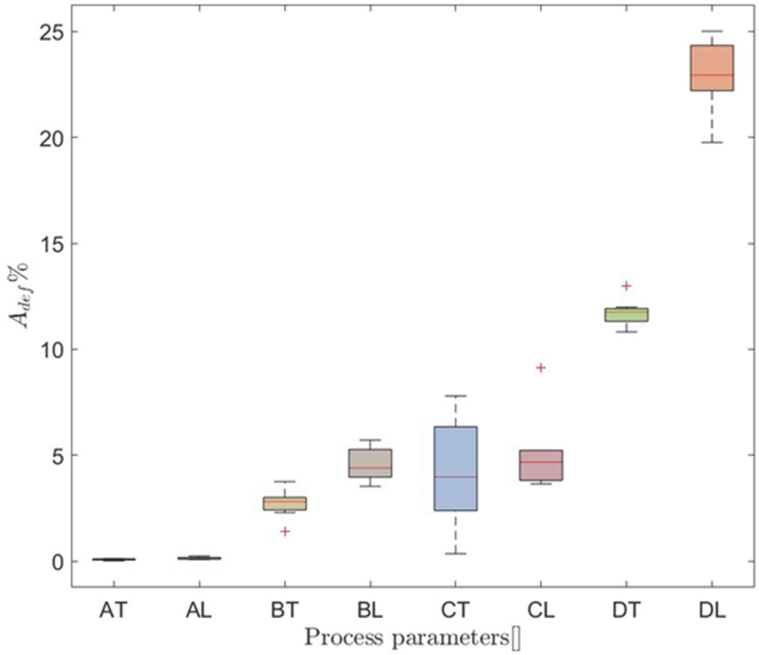

Figure 7: Defect area percentage for each set of printing parameters (A, B, C, and D), measured on longitudinal (L) and transverse (T) sections relative to the build direction.

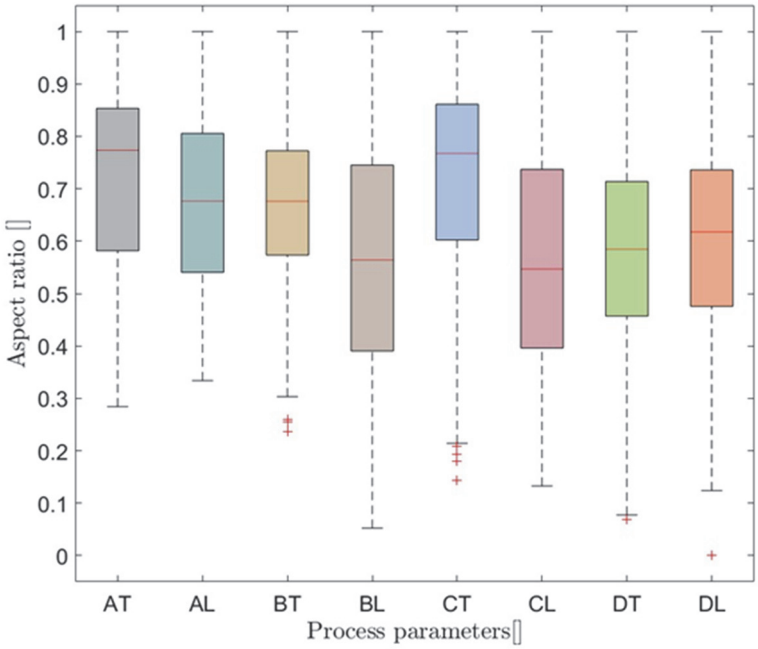

Figure 8: Aspect ratio for each set of printing parameters (A, B, C, and D), measured along longitudinal (L) and transverse (T) sections relative to the build direction.

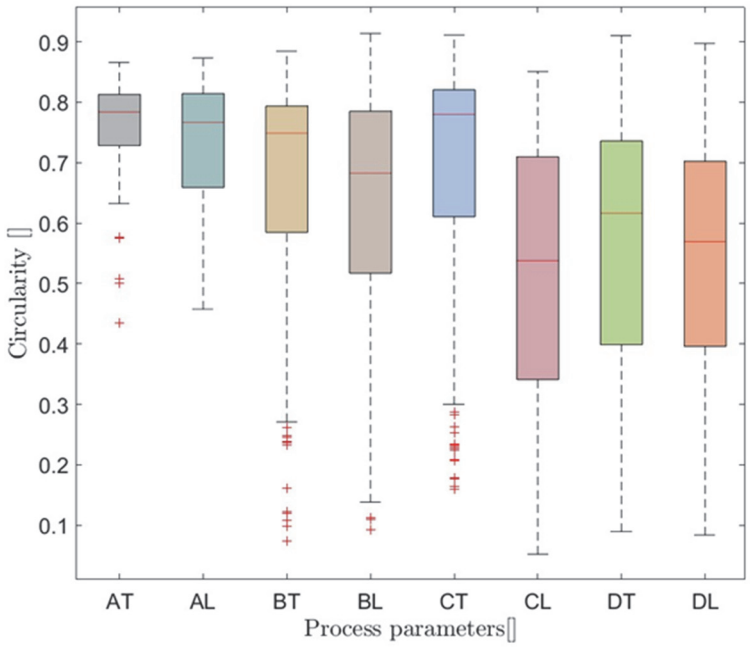

Figure 9: Circularity for each set of printing parameters (A, B, C, and D), measured along longitudinal (L) and transverse (T) sections relative to the build direction.

At the same time, both the circularity and the Feret diameter of CL are higher than BL, maintaining the same percentage of area occupied by defects. It indicates that C has defects with more complex shape and higher dimensions compared to B along the longitudinal section.
Batch A shows the smallest defects of all the batches: Feret diameter ranging from 4 μm to 103 μm, with 50% of the dataset within 8-21μm. Their size combined with the high circularity and aspect ratio is compatible with gas pores.

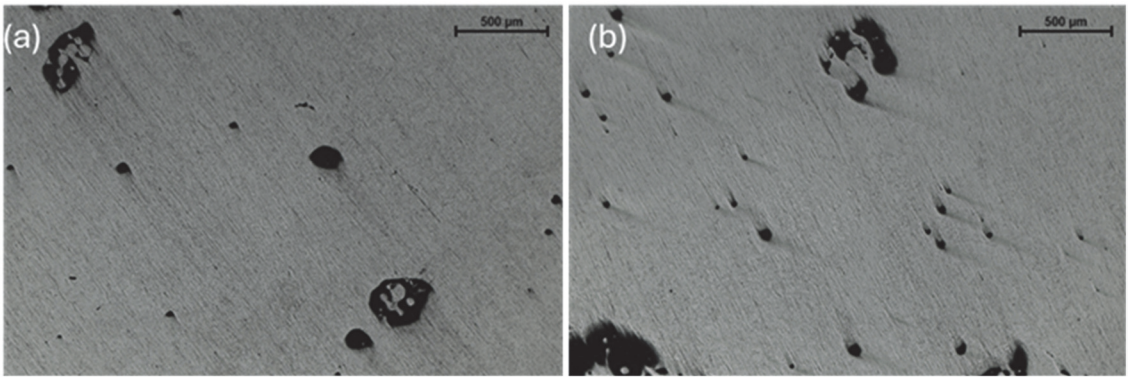

Figure 10: Transverse section of samples B (a) and C (b). The second one shows a higher quantity of gas pores.

To better understand the specimen behavior all fracture surfaces have been observed by SEM. The micrographs in Fig. 11 show that specimen A is characterized by a ductile behavior regardless of the build direction. White arrows in Fig. 11 (b) indicate that, when the sample is loaded perpendicularly to the build direction, the different layers elongate and show a lateral contraction, determining a sort of delamination between adjacent layers.
As already pointed out when discussing stress-strain curves, samples B and C exhibit very similar behavior. Fig. 12 shows that in these specimens, the presence of lack of fusion defects determines the material's behavior. In fact, when the specimen is built vertically, the fracture propagates through the lack of fusion defects: the fracture surface is characterized by the presence of smooth areas, which correspond to the surfaces of the lack of fusion defects, and by actual fracture surfaces characterized by the presence of dimples (Fig. 12(a)). When the specimen is instead built horizontally, the fracture surface of the tensile specimen shows a large area with the presence of dimples, and delamination between adjacent layers is observed (white arrows in Fig. 12 (b)), caused by the lateral contraction of the individual layers during deformation [22-24].

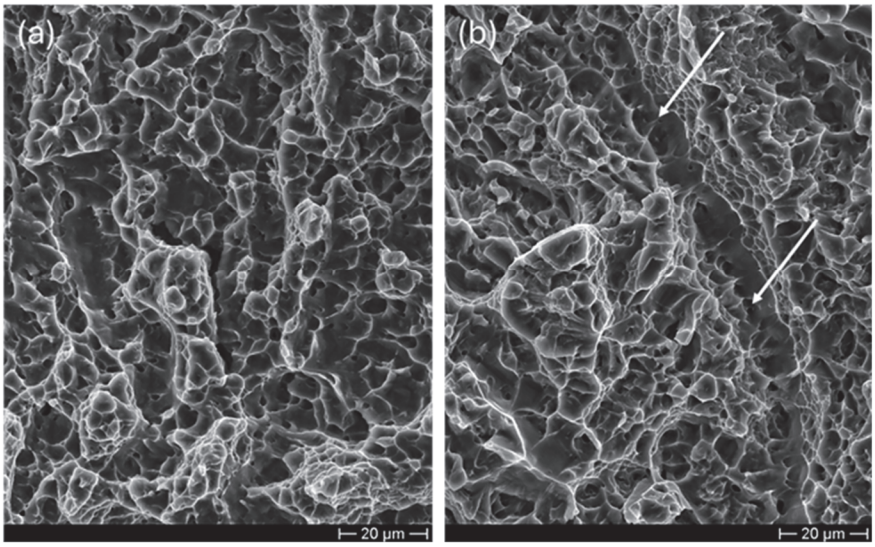

Figure 11: SEM micrographs showing the fracture surface morphology of samples AV (a) and AH (b).

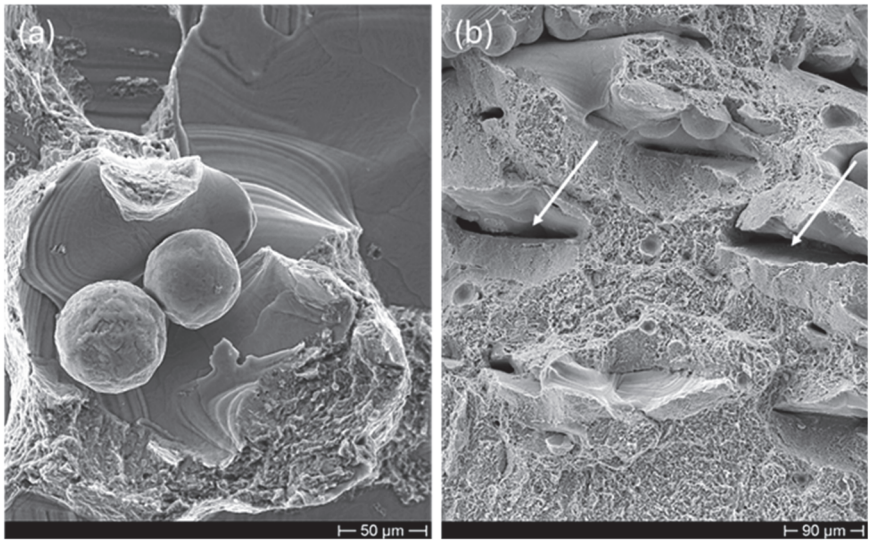

Figure 12: SEM micrograph showing the fracture surface morphology of samples BV (a) and BH (b).

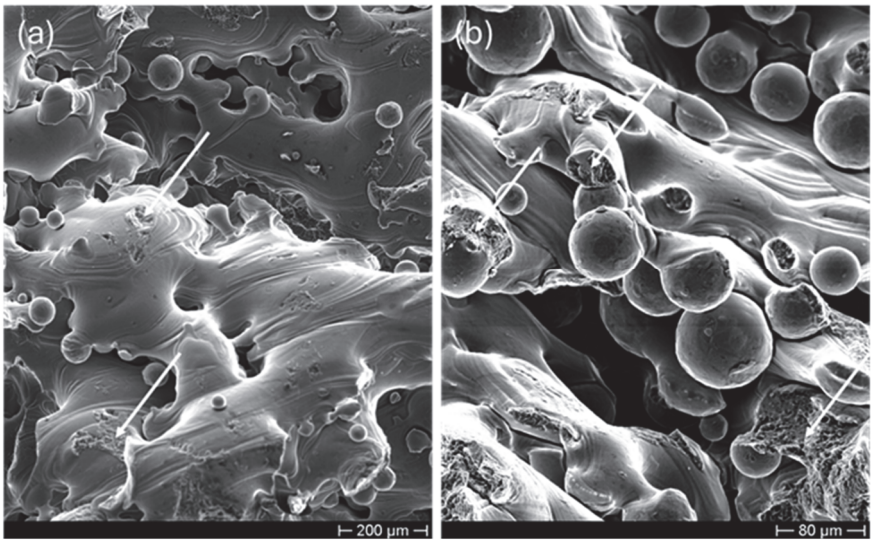

Figure 13: SEM micrographs showing the fracture surface morphology of samples DV (a) and DH (b).

As we noticed when analyzing the tensile curves, sample D exhibits the poorest strength properties. The SEM micrographs shown in Fig. 13 reveal that almost the entire surface is characterized by smooth areas corresponding to lack of fusion defects and the presence of unmelted powder particles. The white arrows, on the other hand, indicate some of the actual fracture surfaces characterized by dimples. As can be observed in the figure, the load-bearing surface for sample D is very small. This justifies the material behavior. All these results allow us to understand the mechanical behavior of Ti6Al4V parts processed by using EBM and to tailor the mechanical behavior by selecting the most appropriate process parameters.

Conclusions

The research reported in this paper is part of a broader research project and aims at investigating the relationship between process parameters used during EBM fabrication of Ti6Al4V parts and the alloy mechanical properties. Process parameters affect microstructural evolution, defect formation, and then the mechanical performance of the alloy. The results highlighted that, when the selected volumetric energy density is sufficient to ensure the production of a dense part, the mechanical properties of the alloy are comparable to those of the alloy produced using traditional techniques. Furthermore, it has been observed that the building direction, in the case of a dense material, does not appear to significantly affect the mechanical properties, although columnar growth of prior beta grains occurs. On the contrary, if the process parameters lead to the formation of defects, particularly lack of fusion defects, the direction of load application relative to the building direction significantly affects the mechanical behavior of the alloy. This has been explained considering that lack of fusion defects are characterized by different morphology on the section parallel and on the section perpendicular to the building direction. The results revealed that on the longitudinal sections defects are characterized by a lower circularity and by a lower aspect ratio. Consequently, when the loading direction is parallel to the building direction, defects exhibiting a low radius of curvature act as stress concentrators to a greater extent, thereby significantly reducing the mechanical strength of the component.

Acknowledgements

This research was funded by the European Union- Next Generation EU, Mission 4 Component 1 CUP B53D23005680006.

References

[1] Bartolomeu F., Gasik M., Silva F.S., Miranda G. (2022). Mechanical properties of Ti-6Al-4V fabricated by laser powder bed fusion: a review focused on the processing and microstructural parameters influence on the final properties. Metals 12, 986. DOI: https://doi.org/10.3390/met12060986.

[2] Nguyen H.D., Pramanik A., Basak A.K., Dong Y., Prakash C., Debnath S. et al. (2022). A critical review on additive manufacturing of Ti-6Al-4V alloy: microstructure and mechanical properties. Journal of Materials Research and Technology, 18, pp. 4641-4661. DOI: https://doi.org/10.1016/j.jmrt.2022.04.055.

[3] Del Guercio G., Galati M., Saboori A., Fino P., Iuliano L. (2020). Microstructure and mechanical performance of Ti-6Al-4V lattice structures manufactured via electron beam melting (EBM): a review. Acta Metallurgica Sinica (English Letters), 33, pp. 183-203. DOI: https://doi.org/10.1007/s40195-020-00998-1.

[4] Gong X., Anderson T., Chou K. (2014). Review on powder-based electron beam additive manufacturing technology. Manufacturing Review 1, 2. DOI: https://doi.org/10.1051/mfreview/2014001.

[5] Bruno J., Rochman A., Cassar G. (2017). Effect of build orientation of electron beam melting on microstructure and mechanical properties of Ti-6Al-4V. Journal of Materials Engineering and Performance, 26, pp. 692-703. DOI: https://doi.org/10.1007/s11665-017-2502-4.

[6] Buhairi M.A., Foudzi F.M., Jamhari F.I. et al. (2023). Review on volumetric energy density: influence on morphology and mechanical properties of Ti-6Al-4V manufactured via laser powder bed fusion. Progress in Additive Manufacturing, 8, pp. 265-283. DOI: https://doi.org/10.1007/s40964-022-00328-0.

[7] Dilip J.J.S., Zhang S., Teng C. et al. (2017). Influence of processing parameters on the evolution of melt pool, porosity, and microstructures in Ti-6Al-4V alloy parts fabricated by selective laser melting. Progress in Additive Manufacturing, 2, pp. 157-167. DOI: https://doi.org/10.1007/s40964-017-0030-2.
[8] Zhang L.C., Liu Y., Li S., Hao Y. (2018). Additive manufacturing of titanium alloys by electron beam melting: a review. Advanced Engineering Materials, 20, 1700842. DOI: https://doi.org/10.1002/adem.201700842.
[9] Carolo L.C.B., Cooper R.E.O. (2022). A review on the influence of process variables on the surface roughness of Ti-6Al-4V by electron beam powder bed fusion. Additive Manufacturing, 59, 103103. DOI: 10.1016/j.addma.2022.103103.
[10] Kan W.H., Chiu L.N.S., Lim C.V.S. et al. (2022). A critical review on the effects of process-induced porosity on the mechanical properties of alloys fabricated by laser powder bed fusion. Journal of Materials Science, 57, pp. 9818-9865. DOI: https://doi.org/10.1007/s10853-022-06990-7.
[11] Sanaei N., Fatemi A. (2021). Defects in additive manufactured metals and their effect on fatigue performance: a state-of-the-art review. Progress in Materials Science, 117, 100724. DOI: https://doi.org/10.1016/j.pmatsci.2020.100724.
[12] Montalbano T., Casagrande T., Gheller A. et al. (2021). Uncovering the coupled impact of defect morphology and microstructure on the tensile behavior of Ti-6Al-4V fabricated via laser powder bed fusion. Journal of Materials Processing Technology, 294, 117113. DOI: https://doi.org/10.1016/j.jmatprotec.2021.117113.
[13] Tammas-Williams S., Zhao H., Léonard F., Derguti F., Todd I., Prangnell P.B. (2015). XCT analysis of the influence of melt strategies on defect population in Ti-6Al-4V components manufactured by selective electron beam melting. Materials Characterization, 102, pp. 47-61. DOI: https://doi.org/10.1016/j.matchar.2015.02.008.
[14] Bergant M.A., Soria S.R., Bustos R.I., Soul H.R., Yawny A.A. (2025). On the relative significance of roughness, printing defects and microstructure on the fatigue behavior of electron beam melted Ti-6Al-4V. Fatigue & Fracture of Engineering Materials & Structures, 48, in-press. DOI: https://doi.org/10.1111/ffe.14565.
[15] Thalavai Pandian K., Lindgren E., Roychowdhury S. et al. (2024). Characterization of surface asperities to understand its effect on fatigue life of electron beam powder bed fusion manufactured Ti-6Al-4V. International Journal of Fatigue, 188, 108516. DOI: https://doi.org/10.1016/j.ijfatigue.2024.108516.
[16] Batalha G.F., Pardal G., Peres R.A. et al. (2024). Mechanical properties characterization of Ti-6Al-4V grade 5 (recycled) additively manufactured by selective electron beam melting (EB-PBF). Engineering Failure Analysis, 157, 107892. DOI: https://doi.org/10.1016/j.engfailanal.2023.107892.
[17] Bradski G. (2000). The OpenCV library. Dr. Dobb's Journal of Software Tools (2000).
[18] Neikter M., Åkerfeldt P., Pederson R., Antti M.L., Sandell V. (2018). Microstructural characterization and comparison of Ti-6Al-4V manufactured with different additive manufacturing processes. Materials Characterization, 143, pp. 68-75. DOI: https://doi.org/10.1016/j.matchar.2018.02.003.
[19] Al-Bermani S.S., Blackmore M.L., Zhang W., Todd I. (2010). The origin of microstructural diversity, texture, and mechanical properties in electron beam melted Ti-6Al-4V. Metallurgical and Materials Transactions A, 41, pp. 3422-3434. DOI: https://doi.org/10.1007/s11661-010-0397-x.
[20] Yuan L., Ding S., Wen C. (2019). Additive manufacturing technology for porous metal implant applications and triply periodic minimal surface structures: a review. Bioactive Materials, 4, pp. 56-70. DOI: 10.1016/j.bioactmat.2018.12.003.
[21] Gibson L.J., Ashby M.F., (1997). Cellular Solids: Structure and Properties (2nd ed.). Cambridge University Press, Cambridge.
[22] Sarparast, M., Shafaie, M., Davoodi, M., Memaran Babakan, A. and Zhang, H. (2024). Predictive Modeling of Fracture Behavior in Ti6Al4V Alloys Manufactured by SLM Process. Fracture and Structural Integrity, 18(68), pp. 340–356. DOI: https://doi.org/10.3221/IGF-ESIS.68.23.
[23] Navarro Pintado, C., Vázquez, J., Domínguez, J., Periñán, A., Herrera García, M., Lasagni, F., Bernardin, S., Slawik, S., Mucklich, F., Boby, F. and Hackel, L. (2020). Effect of surface treatment on the fatigue strength of additive manufactured Ti6Al4V alloy. Fracture and Structural Integrity, 14(53), pp. 337–344. DOI: https://doi.org/10.3221/IGF-ESIS.53.26.
[24] Yarullin, R. and Yakovlev, M. (2022). Fatigue growth rate of inclined surface cracks in aluminum and titanium alloys. Fracture and Structural Integrity, 16(60), pp. 451–463. DOI: https://doi.org/10.3221/IGF-ESIS.60.31.